

Spoofting Attack Detection in the Physical Layer with Robustness to User Movement

Daniel Romero

Department of ICT, University of Agder

Grimstad, Norway

daniel.romero@uia.no

Tien Ngoc Ha

Department of ICT, University of Agder

Grimstad, Norway

tien.n.ha@uia.no

Peter Gerstoft

UC San Diego

San Diego, USA

pgerstoft@ucsd.edu

Abstract—In a spoofing attack, an attacker impersonates a legitimate user to access or modify data belonging to the latter. Typical approaches for spoofing detection in the physical layer declare an attack when a change is observed in certain channel features, such as the received signal strength (RSS) measured by spatially distributed receivers. However, since channels change over time, for example due to user movement, such approaches are impractical. To sidestep this limitation, this paper proposes a scheme that combines the decisions of a position-change detector based on a deep neural network to distinguish spoofing from movement. Building upon community detection on graphs, the sequence of received frames is partitioned into subsequences to detect concurrent transmissions from distinct locations. The scheme can be easily deployed in practice since it just involves collecting a small dataset of measurements at a few tens of locations that need not even be computed or recorded. The scheme is evaluated on real data collected for this purpose.

Index Terms—Spoofting attack, physical layer security, deep learning, community detection, cybersecurity, wireless networks.

I. INTRODUCTION

The shared nature of the wireless communication channel opens the door for a large number of attacks that seek to illicitly obtain private data, compromise the uptime of remote services, or impersonate other users [1]–[4]. Spoofting attacks, which pursue the latter goal, are especially problematic since they endow the attacker with the capacity to access and modify data intended for or produced by a legitimate user. Detecting these attacks is therefore vital to guarantee data security.

Cryptographic techniques can be employed at one or multiple communication layers to preempt spoofing attacks. However, these security barriers are readily bypassed by an attacker with the user credentials. For this reason, techniques to detect spoofing attacks in the physical layer have been developed, typically by exploiting physical layer characteristics that are specific to the transmitter, such as the carrier frequency offset (CFO), or channel features, such as the received signal strength (RSS) or Angle of Arrival (AoA).

More specifically, CFO, I/Q offset, and I/Q imbalance were used to verify user identity in [5]–[8]. Unfortunately, these techniques necessitate knowledge of the communication protocol and may fail under changes in the environment; e.g.

in temperature [6]. These limitations have been partially alleviated in [9]–[11], which employ AoA and TDoA features, and in [12], where a neural network is trained on signal-to-noise ratio (SNR) traces. However, they still require synchronization and/or knowledge of the communication protocol.

In comparison, RSS-based techniques need not know the protocols or decode signals, which greatly enhances their generality and applicability for spoofing detection [13]–[17]. The most common technique in this context applies K-means to RSS measurements collected by multiple receivers [13], [18], [19]. Leveraging the dependence of RSS signatures on the location of the transmitter, an attack is declared iff transmissions with the same user ID originate at different locations. This means that attacks are declared *even when the channel changes*, which occurs e.g. when a user moves.

Fortunately, it is possible to tell spoofing from motion and other changes by looking at the nature of the changes. To see this, suppose that a network sequentially receives frames from points A, B, C, and D. If all these points are different, it is natural to ascribe these changes to user movement. On the contrary, if the transmissions are received from points A, B, A, B, A, B, etc., it is likely that one user is transmitting from A and another from B, thereby suggesting the presence of an attack. However, to our knowledge, no existing algorithm leverages this kind of information.

This paper fills this gap by developing an RSS-based spoofing attack detector that builds upon the aforementioned observation. The main contribution is a two-tier scheme where the decisions of a low-level *position-change detector* (PCD), such as the detectors alluded to earlier, are combined by a higher-level algorithm to detect the presence of concurrent transmissions from different locations. To simplify the terminology, the exposition assumes that all changes are due to user movement, but the algorithm carries over without modification to changes caused by other factors such as the movement of scatterers or obstructions. The high-level algorithm invokes a graph community detection primitive to decompose the received frame sequence into subsets corresponding to the same location. Since existing PCDs necessitate accurate RSS estimates, which requires long averaging time, a secondary contribution is a PCD based on a deep neural network (DNN) that provides a higher spatiotemporal resolution by learning the distribution of coarse RSS estimates.

This research has been funded in part by the Research Council of Norway under IKTPLUSS grant 311994.

The datasets and code are available at <https://github.com/fachu000/spoofting>.

Collecting data for deploying the proposed algorithm is remarkably simple: it just involves recording samples for a few tens of transmitter locations. As opposed to related algorithms, such as those for fingerprinting localization, locations need not be computed or recorded, which greatly simplifies the process.

II. MODEL AND PROBLEM FORMULATION

Let $\mathcal{X} \subset \mathbb{R}^3$ comprise the coordinates of all points in the spatial region of interest, where both legitimate users and attackers are located. A transmitter at $\mathbf{x} \in \mathcal{X}$ transmits a signal with complex baseband representation $s(t)$, where t denotes time. This signal, modeled as an unknown wide-sense stationary stochastic process, is received by N static receivers, which may be e.g. access points or base stations. After downconversion, the signal at the n th receiver is

$$r_n(\mathbf{x}, t) = h_n(\mathbf{x}, t) * s(t) + z_n(t), \quad (1)$$

where $*$ denotes convolution, $h_n(\mathbf{x}, t)$ is the unknown deterministic impulse response of the bandpass equivalent channel between \mathbf{x} and the n th receiver, and $z_n(t)$ is noise. As usual, $z_n(t)$ is assumed wide-sense stationary and uncorrelated with $s(t)$. Thus, one can define the *received signal strength* (RSS) $f_n^{\text{true}}(\mathbf{x}) := \mathbb{E}|r_n(\mathbf{x}, t)|^2$, where \mathbb{E} denotes expectation. To estimate $f_n^{\text{true}}(\mathbf{x})$, the n th receiver averages the square magnitude of K samples $\{|r_n(\mathbf{x}, kT)|^2\}_k$, where T is the sampling interval. If $r_n(\mathbf{x}, kT)$ is ergodic for each \mathbf{x} , it follows that $f_n(\mathbf{x})$ converges to $f_n^{\text{true}}(\mathbf{x})$ as $K \rightarrow \infty$. This number of averaged samples K will play an important role in Sec. III-A.

A fusion center forms the RSS vector estimate $\mathbf{f}(\mathbf{x}) := [f_0(\mathbf{x}), \dots, f_{N-1}(\mathbf{x})]^\top$ by gathering these N RSS estimates. It is assumed that the position \mathbf{x} of the transmitter does not change significantly during the process of acquiring these estimates, which is a mild assumption if K is small, as considered here. Repeating this operation for each of a collection of J consecutive received frames results in the frame sequence $\mathbf{F} := [\mathbf{f}[0], \dots, \mathbf{f}[J-1]]$, where $\mathbf{f}[j] := \mathbf{f}(\mathbf{x}[j])$ and $\mathbf{x}[j] \in \mathcal{X}$ is the location of the user that transmitted the j th frame at the transmission time.

Out of these J frames, some belong to the legitimate user whereas others may belong to the attacker. Let $\mathcal{J}_L \subset \{0, \dots, J-1\}$ contain the indices of the frames transmitted by the legitimate user and let $\mathcal{J}_A := \{0, \dots, J-1\} - \mathcal{J}_L$ contain the indices of the frames transmitted by the attacker. Given \mathbf{F} , the problem is to decide between the following hypotheses:

$$\begin{cases} \mathcal{H}_0^{\text{SD}} : \mathcal{J}_A = \emptyset \\ \mathcal{H}_1^{\text{SD}} : \mathcal{J}_A \neq \emptyset. \end{cases} \quad (2)$$

To assist in this task, a data set of feature vectors $\{\mathbf{f}^{(i)}(\mathbf{x}_m), m = 0 \dots M-1, i = 0, \dots, I-1\}$ is given, where $\mathbf{x}_m \neq \mathbf{x}_{m'}$ for all $m \neq m'$ and $\{\mathbf{f}^{(i)}(\mathbf{x}_m)\}_{i=0}^{I-1}$ denote I estimates of $\mathbf{f}^{\text{true}}(\mathbf{x}_m) := [f_0^{\text{true}}(\mathbf{x}_m), \dots, f_{N-1}^{\text{true}}(\mathbf{x}_m)]^\top$.

III. DNN-BASED SPOOFING DETECTOR

Clearly, if each $\mathbf{f}[j]$ is transmitted from a totally different location, possibly far from $\mathbf{f}[j-1]$ and $\mathbf{f}[j+1]$, then there

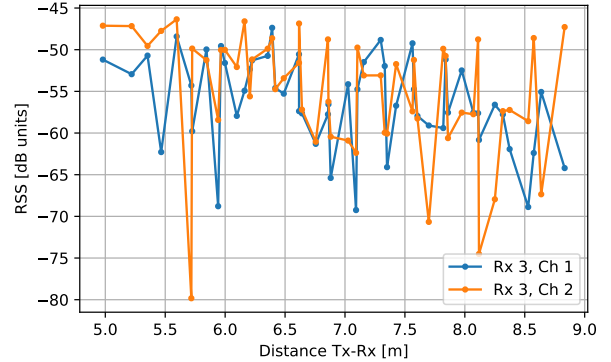


Fig. 1: RSS vs. distance for two of the 16 channels in the dataset. It is observed that small distance changes may result in larger RSS changes than large distance changes.

is no hope of reasonably solving (2) since the possible distributions of \mathbf{F} are the same under $\mathcal{H}_0^{\text{SD}}$ and $\mathcal{H}_1^{\text{SD}}$. Thus, the following assumption is required:

(As1) The frame rate is high relative to the speed of the users.

In other words, the movement of the users between two consecutive frames is not too large, or, more precisely, $\mathbf{x}[j]$ is close to $\mathbf{x}[j-1]$ if both $j-1$ and j are in either \mathcal{J}_L or \mathcal{J}_A .

Based on this assumption, one could attempt to solve (2) by first estimating $\mathbf{x}[j]$ from $\mathbf{f}[j]$ for each j and then deciding that two consecutive frames belong to the same user if the corresponding location estimates are nearby. However, this approach is not viable because (i), as per the problem formulation in Sec. II, the locations are not part of the data, and (ii), even if the locations were given, estimating $\mathbf{x}[j]$ entails a large error. This is seen from Fig. 1, which shows $f_n(\mathbf{x})$ obtained with a large K for two values of n vs. the distance from \mathbf{x} to the n th receiver in the setup of Sec. IV. It is seen that small distance changes often result in larger RSS changes than large distance changes. In other words, for this room, the multipath variability in the channel is larger than the path-loss variability. Consequently, the error in estimating $\mathbf{x}[j]$ from $\mathbf{f}[j]$ can be seen to be in the order of the room size, which renders such estimates useless. Estimating $\mathbf{x}[j]$ with a sufficient accuracy would require more complex features.

Instead, this paper relies on a PCD which decides whether each pair of frames were transmitted from the same location or not, a much coarser form of information than $\mathbf{x}[j]$. Based on the PCD decisions, a *spoofing detector* (SD) decides $\mathcal{H}_0^{\text{SD}}$ or $\mathcal{H}_1^{\text{SD}}$. Although existing algorithms can be used as PCDs, Sec. III-A proposes one especially attuned to low values of K . Afterwards, Sec. III-B presents the proposed SD.

A. Position-Change Detector

This section considers the subproblem of determining whether two frames were transmitted from the same location. Specifically, given the estimates $\mathbf{f}(\mathbf{x}_1)$ and $\mathbf{f}(\mathbf{x}_2)$ corresponding to the (potentially equal) locations $\mathbf{x}_1, \mathbf{x}_2 \in \mathcal{X}$, the

problem is to decide between the following hypotheses:

$$\begin{cases} \mathcal{H}_0^{\text{PCD}} : \mathbf{x}_1 = \mathbf{x}_2 \\ \mathcal{H}_1^{\text{PCD}} : \mathbf{x}_1 \neq \mathbf{x}_2. \end{cases} \quad (3)$$

A PCD is a function $d^{\text{PCD}} : \mathbb{R}^N \times \mathbb{R}^N \rightarrow \{\mathcal{H}_0^{\text{PCD}}, \mathcal{H}_1^{\text{PCD}}\}$ that returns one of these hypotheses for each pair $(\mathbf{f}, \mathbf{f}')$.

Existing algorithms (cf. Sec. I) assume a sufficiently large K , which limits temporal resolution. In contrast, this section proposes a PCD that affords a low K by using a DNN that learns the distribution of the feature vector *estimates*.

1) *Data Set*: The training dataset is constructed to comprise $2P$ pairs $\{(\mathbf{f}^{(i_p)}(\mathbf{x}_{m_p}), \mathbf{f}^{(i'_p)}(\mathbf{x}_{m'_p}))\}_{p=0}^{2P-1} \subset \mathbb{R}^N \times \mathbb{R}^N$. For the first P pairs, $m_p = m'_p$ (so $\mathcal{H}_0^{\text{PCD}}$ holds), whereas for the last P pairs, $m_p \neq m'_p$ (so $\mathcal{H}_1^{\text{PCD}}$ holds). For the p th pair, $p = 0, \dots, 2P - 1$, the indices i_p and i'_p are drawn uniformly at random without replacement from $\{0, \dots, I - 1\}$. For $p = 0, \dots, P - 1$, index $m_p = m'_p$ is drawn uniformly at random from $\{0, \dots, M - 1\}$. For $p = P, \dots, 2P - 1$, indices m_p and m'_p are drawn uniformly at random without replacement from $\{0, \dots, M - 1\}$.

2) *Architecture*: Detectors are typically designed to decide $\mathcal{H}_1^{\text{PCD}}$ if $T^{\text{PCD}}(\mathbf{f}, \mathbf{f}')$ exceeds a threshold and $\mathcal{H}_0^{\text{PCD}}$ otherwise, where function $T^{\text{PCD}} : \mathbb{R}^N \times \mathbb{R}^N \rightarrow \mathbb{R}$ is a *detection statistic*. This can be directly implemented as a DNN.

However, to boost detection performance, it is worth applying a technique to make the detector commutative. Specifically, if T^{PCD} is just a generic DNN, it will generally occur that $T^{\text{PCD}}(\mathbf{f}, \mathbf{f}') \neq T^{\text{PCD}}(\mathbf{f}', \mathbf{f})$, which is inconsistent with the symmetry of (3). To remedy this, the proposed PCD uses a DNN to implement an auxiliary function \tilde{T}^{PCD} and then sets $T^{\text{PCD}}(\mathbf{f}, \mathbf{f}') = (\tilde{T}^{\text{PCD}}(\mathbf{f}, \mathbf{f}') + \tilde{T}^{\text{PCD}}(\mathbf{f}', \mathbf{f}))/2$. It can be seen that $T^{\text{PCD}}(\mathbf{f}, \mathbf{f}') = T^{\text{PCD}}(\mathbf{f}', \mathbf{f})$ and that the 2 in the denominator can be absorbed into $\tilde{T}^{\text{PCD}}(\mathbf{f}, \mathbf{f}')$.

Function \tilde{T}^{PCD} is implemented as a feed-forward network whose first layer is non-trainable and produces $10 \log_{10}[\|\mathbf{f}, \mathbf{f}', \mathbf{f} - \mathbf{f}'\|]$ when the network input is $[\mathbf{f}, \mathbf{f}']$. The subsequent 3 hidden layers are fully connected with leaky ReLU activations and 512 neurons [20]. The output layer is fully connected with a single neuron with linear activation.

3) *Training*: The DNN is trained using a binary cross-entropy loss with ℓ_1 -regularization. A subset of M_{val} points are set apart for validation and the remaining $M_{\text{tr}} := M - M_{\text{val}}$ are used for training. The procedure in Sec. III-A1 is applied separately to each subsets by setting M and P respectively to M_{tr} and P_{tr} for training and to M_{val} and P_{val} for validation.

B. Spoofing Detector

The PCD is applied to all pairs of frames to obtain the decisions $d[j, j'] := d^{\text{PCD}}(\mathbf{f}[j], \mathbf{f}[j'])$. The question is how to combine these decisions to choose between $\mathcal{H}_0^{\text{SD}}$ and $\mathcal{H}_1^{\text{SD}}$. To this end, this section proposes a decision rule $d^{\text{SD}} : \mathbb{R}^{N \times J} \rightarrow \{\mathcal{H}_0^{\text{SD}}, \mathcal{H}_1^{\text{SD}}\}$ based on the notion of *region*. For didactical purposes, this concept is first introduced in an ideal scenario.

A *region* $\mathcal{R} \subset \{0, \dots, J - 1\}$ is a *set of indices* such that $d[j, j'] = \mathcal{H}_0^{\text{PCD}}$ for all $j, j' \in \mathcal{R}$ whereas $d[j, j'] = \mathcal{H}_1^{\text{PCD}}$

if $j \in \mathcal{R}$ and $j' \notin \mathcal{R}$ (or vice versa since $d[j, j'] = d[j', j] \forall j, j'$). Note that, as per this definition, this is not a geometric notion. However, the term *region* was chosen since one can intuitively identify each region with a spatial area where the channel is roughly constant to the eyes of d^{PCD} .

With this in mind, consider the following assumption:

(As2) The frame sequence can be partitioned into regions.

In other words, (As2) states that, for each frame sequence \mathbf{F} , there is a collection of regions such that each frame $\mathbf{f}[j]$ belongs to one and only one region. However, the above definition of region is too strict for (As2) to hold in general, but analyzing simple cases offers insight that will be used to relax the notion of region so that (As2) holds.

Consider first a single legitimate user that remains static and assume that all PCD decisions are correct. Since $d[j, j'] = \mathcal{H}_0^{\text{PCD}}$ for all j, j' , all frames belong to the same region $\mathcal{R} = \{0, \dots, J - 1\}$. With two static users, one being the attacker, $d[j, j'] = \mathcal{H}_0^{\text{PCD}}$ if $j, j' \in \mathcal{J}_L$ or $j, j' \in \mathcal{J}_A$, and $d[j, j'] = \mathcal{H}_1^{\text{PCD}}$ otherwise. Thus, one can set $\mathcal{R}_1 = \mathcal{J}_L$ and $\mathcal{R}_2 = \mathcal{J}_A$.

Consider now a single user at one location up to frame j_0 and at another location from frame $j_0 + 1$ on. Then $\mathcal{R}_1 = \{0, \dots, j_0\}$ and $\mathcal{R}_2 = \{j_0 + 1, \dots, J - 1\}$. This observation, which is extensible to an arbitrary number of spatial locations, constitutes a discretization of the user movement but can be made arbitrarily accurate by increasing the number of considered points and its impact will be mitigated once the definition of region is relaxed. The cases of two moving users or a static user and a moving user can be handled similarly.

To illustrate these cases, Fig. 2 shows examples of *region sequences*, namely sequences of indices $r[0], \dots, r[J - 1]$ where $r[j]$ is the index of the region to which frame j belongs, i.e., $j \in \mathcal{R}_{r[j]} \forall j$. Note that region indices are arbitrary.

While (As2) holds in the above ideal scenarios, it will not generally hold. The next section copes with this issue.

1) *Region Estimation via Community Detection*: The reason why it is not generally possible to decompose the frame sequence as a disjoint union of regions is that d^{PCD} is not generally *transitive*, which means that even though $d^{\text{PCD}}(\mathbf{f}, \mathbf{f}') = d^{\text{PCD}}(\mathbf{f}', \mathbf{f}'') = \mathcal{H}_0^{\text{PCD}}$, it may happen that $d^{\text{PCD}}(\mathbf{f}, \mathbf{f}'') = \mathcal{H}_1^{\text{PCD}}$. This may be caused by noise or other factors. However, given (As1), one expects that transitivity is violated only for a few frames, a fact exploited next.

Consider a graph \mathcal{G} where each node corresponds to a frame and there is an edge between node j and node j' iff $d[j, j'] = \mathcal{H}_0^{\text{PCD}}$. A decomposition of a frame sequence into regions induces a decomposition of the graph into *fully-connected components*. Recall that the latter comprise sets of nodes that are connected to each other but not to any other node outside the component [21, Ch. 2]. This notion can be relaxed into that of *community*. A community informally refers to a set of nodes with a large number of edges between them and few edges to nodes outside the community [21, Sec. 4.3.3]. The term is coined in analogy to a community in a social network, e.g., a group of friends. Algorithms to determine the communities of a graph abound and are referred to as

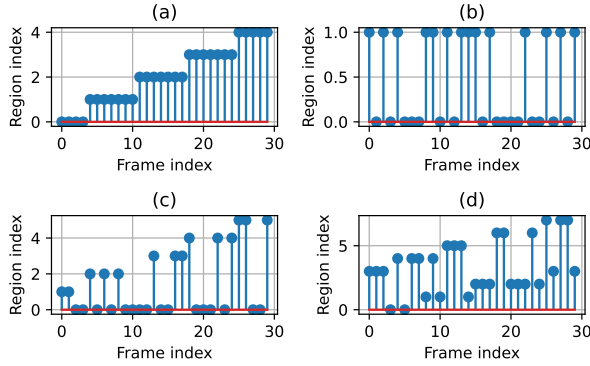


Fig. 2: Examples of region sequences. (a) Single moving transmitter. (b) Two static transmitters. (c) Two transmitters, one is static and the other moves. (d) Two moving transmitters.

community detection algorithms. A popular one is the *Louvain method*, which optimizes a metric called *modularity* [22].

The proposed method takes \mathbf{F} as input and constructs the adjacency matrix of \mathcal{G} by evaluating d^{PCD} for all $\mathbf{f}[j]$ and $\mathbf{f}[j']$ with $j < j'$. The Louvain method is then applied to partition the graph into communities, which yields a sequence $r[0], \dots, r[J-1]$ with the indices of the community corresponding to each frame. This sequence will still be referred to as a region sequence although, strictly speaking, each community does not exactly correspond to a region according to the definition of region at the beginning of Sec. III-B. However, it may be identified with a region in a softer sense, since a community may miss a few edges inside or may have edges to nodes outside.

2) *Decision Rule:* Having determined $r[0], \dots, r[J-1]$, the final step is to decide $\mathcal{H}_0^{\text{SD}}$ or $\mathcal{H}_1^{\text{SD}}$. This process comprises two steps: first, a test statistic T^{SD} is evaluated. Then, this statistic is compared with a threshold γ^{SD} to decide $\mathcal{H}_1^{\text{SD}}$ if $T^{\text{SD}}(r[0], \dots, r[J-1]) > \gamma^{\text{SD}}$ and $\mathcal{H}_0^{\text{SD}}$ otherwise. Thus, it remains only to find a suitable T^{SD} .

Clearly, T^{SD} should generally take larger values under $\mathcal{H}_1^{\text{SD}}$ than under $\mathcal{H}_0^{\text{SD}}$. Since a sequence with no transitions ($r[j] = r[j']$ for all j, j') would likely correspond to $\mathcal{H}_0^{\text{SD}}$, it follows that T^{SD} must be small in this case. On the other hand, transitions (i.e., indices j such that $r[j] \neq r[j+1]$) indicate either movement or the presence of an attack. Thus, a natural T^{SD} is the number of transitions likely caused by an attack. To distinguish both kinds of transitions, observe from Fig. 2 that movement generally results in transitions to regions not visited previously, whereas attack-related transitions revisit regions.

These considerations motivate setting T^{SD} to be the number of transitions to a previously visited region. Specifically, one can write the test statistic as

$$T^{\text{SD}}(r[0], \dots, r[J-1]) = \sum_{j=3}^{J-1} w[j], \quad (4)$$

where $w[j] = 1$ if $r[j] \neq r[j-1]$ and there exists a $j' < j$ such that $r[j] = r[j']$, and $w[j] = 0$ otherwise.

However, due to noise and wrong decisions of d^{PCD} , it is desirable to confer a greater weight to those terms in (4) that correspond to transitions to a *recently* visited region. In particular, if $|\cdot|$ denotes cardinality, then the number of distinct¹ regions visited before returning to $r[j]$ is $\tilde{w}[j] := |\{r[j^*+1], r[j^*+2], \dots, r[j-1]\}|$, where j^* is the largest index such that $j^* < j$ and $r[j^*] = r[j]$. Since an attack is likely to result in low values of $\tilde{w}[j]$, it makes sense to replace $w[j]$ in (4) with $w[j] = 1/\tilde{w}[j]$ if $\tilde{w}[j] \neq 0$ and $w[j] = 0$ otherwise.

The threshold γ^{SD} is then set e.g. to satisfy a target probability of false alarm or to minimize the probability of error.

IV. EXPERIMENTS

This section empirically validates the proposed algorithm using real data. A link to the code and data is provided on the first page.

Several datasets were collected indoors on the campus of the University of California, San Diego. This section focuses on one of those datasets, where a transmitter was sequentially placed at 52 locations along 4 parallel lines. For the sake of reproducibility, the transmitted signal $s(t)$ is a 5 MHz sinusoid at a 2.3 GHz carrier frequency. For every transmitter location, each of the four receivers with four antennas record 4888 samples of the received signal. Thus, N can be set between 1 and $4 \cdot 4 = 16$ by selecting a subset of the receivers and antennas.

The PCD proposed in Sec. III-A, referred to as *DNN-based classifier* (DNNC), is benchmarked with three other PCD algorithms. The first two, termed distance-based classifiers (DBC), decide $\mathcal{H}_1^{\text{PCD}}$ iff $\|\mathbf{f} - \mathbf{f}'\|_q > \gamma^{\text{PCD}}$, where q is 2 for $\text{DBC}(\ell_2)$ and 1 for $\text{DBC}(\ell_1)$. The threshold γ^{PCD} is adjusted to maximize the accuracy over the training pairs. Following [13], [14], the third benchmark is a K-means classifier that clusters the training vectors $\mathbf{f}^{(i)}(\mathbf{x}_m)$ into C clusters. Then it applies the same rule as $\text{DBC}(\ell_2)$ over the two feature vectors that result from collecting the C Euclidean distances from the given \mathbf{f} and \mathbf{f}' to all centroids.

A. Position Change Detection

This section analyzes performance when solving (3). To this end, the adopted metric is the accuracy measured on a test data set comprising the $52 - M$ locations that are not used for training and validation. Recall from Sec. III-A3 that, among these M locations, M_{tr} are used for training and M_{val} for validation. To estimate the accuracy of each algorithm, a new subset of M locations among all 52 available locations is chosen at each Monte Carlo iteration. Also, the DNN weights are randomly initialized at each iteration.

To investigate the number M of training locations that are needed to attain a reasonable accuracy, Fig. 3 (top) depicts accuracy vs. M . It is observed that (i) the accuracy of DNNC is reasonably high with just 45 locations, (ii) DNNC learns much more than the benchmarks with new data.

¹Recall that, due to the definition of *set*, duplicates count as one.

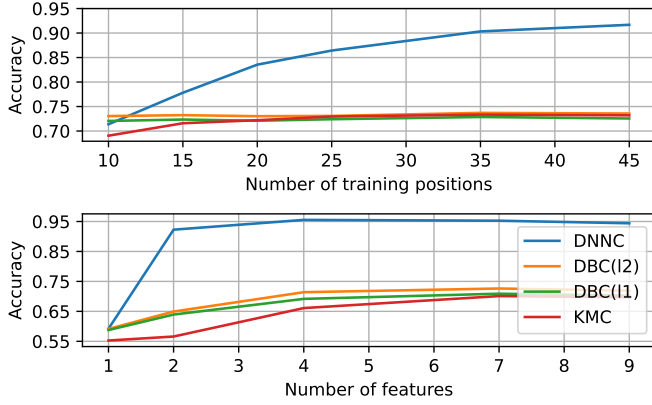


Fig. 3: [Top] Accuracy vs. number of training positions M for the proposed algorithm (DNNC) and the competing algorithms ($K = 16$, $N = 16$, $P_{\text{tr}} = 1250$, $P_{\text{val}} = 150$, $M_{\text{tr}} = 0.8M$, $C = 15$). [Bottom] Accuracy vs. number of features N for DNNC and the competing algorithms ($K = 16$, $P_{\text{tr}} = 1250$, $P_{\text{val}} = 150$, $M = 40$, $M_{\text{tr}} = 0.8M$, $C = 15$).

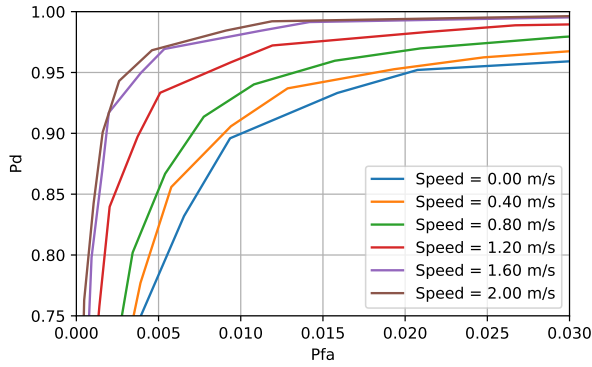


Fig. 4: ROC curves for the proposed SD detector (100 frames/s, $J = 30$, $K = 16$, $N = 16$, $P_{\text{tr}} = 3000$, $P_{\text{val}} = 1000$, $M_{\text{tr}} = 0.8M$).

The second experiment assesses the impact of the number of features. In this data set, the first 4 features correspond to the first receiver, the second 4 features to the second receiver, and so on. Fig. 3 (bottom) shows that two features already result in high accuracy for DNNC. Remarkably, this effect can be seen to be milder when the selected features are obtained by different receivers, suggesting that there is more information in the joint distribution of the RSS estimates from nearby-located antennas than from distant antennas.

In both experiments, only $K = 16$ samples are used, which corroborates that the goal of DNNC to provide high temporal resolution was achieved. Further experiments omitted here show that the accuracy of the benchmarks decreases more abruptly than the one of DNNC if K is reduced below 16.

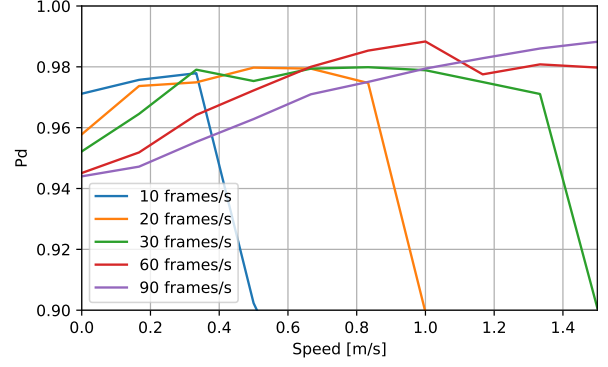


Fig. 5: Probability of detection for a fixed probability of false alarm $P_{\text{FA}} = 0.02$, $J = 20$, $K = 16$, $N = 16$, $P_{\text{tr}} = 3000$, $P_{\text{val}} = 1000$, $M_{\text{tr}} = 0.8M$.

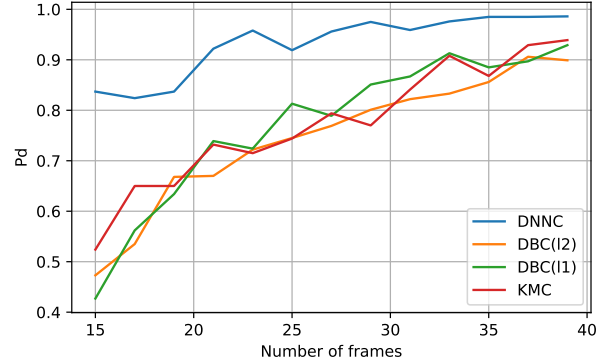


Fig. 6: Probability of detection of spoofing attacks vs. J for different PCDs (10 frames/s, $P_{\text{FA}} = 0.02$, $K = 16$, $N = 16$, $P_{\text{tr}} = 3000$, $P_{\text{val}} = 1000$, $M_{\text{tr}} = 0.8M$).

B. Spoofing Detection

This section studies performance when solving (2). At each Monte Carlo iteration, a frame sequence is generated. Under $\mathcal{H}_0^{\text{SD}}$, the trajectory $\mathbf{x}(t)$ of the (single) user is generated as follows. First, obtain the time duration of the frame sequence, given by JR_J , where R_J is the number of frames per second. The length $\Delta\mathbf{x}$ of the trajectory is therefore $\Delta\mathbf{x} = JR_J v$, where v is the speed of the user. Then, select one of the lines indicated at the beginning of Sec. IV uniformly at random and choose a point $\tilde{\mathbf{x}}$ on that line that is at least $\Delta\mathbf{x}$ from the first and last measurement locations on that line. The trajectory is therefore $\mathbf{x}(t) = \tilde{\mathbf{x}} + \mathbf{d}vt$, where \mathbf{d} is one of the two unit vectors on the selected line chosen uniformly at random. Each $\mathbf{f}[j]$ is obtained using samples in the data set that correspond to the measurement location that lies closest to $\mathbf{x}(j/R_J)$.

Under $\mathcal{H}_1^{\text{SD}}$, the frame sequences of both users are also generated following this procedure. Then, the frame sequence $\mathbf{f}_1[0], \dots, \mathbf{f}_1[J-1]$ of user-1 is merged with the frame sequence $\mathbf{f}_2[0], \dots, \mathbf{f}_2[J-1]$ of user-2 into a sequence $\mathbf{f}[0], \dots, \mathbf{f}[J-1]$ where either $\mathbf{f}[j] = \mathbf{f}_1[j]$ or $\mathbf{f}[j] = \mathbf{f}_2[j]$,

both with probability 1/2 and independently along j .

Fig. 4 presents the *receiver operating characteristic* (ROC) curves [23, Ch. 3] for the test in (2) when the SD from Sec. III-B is used. Observe the large probability of detection (P_D) that is attained with low probability of false alarm (P_{FA}). Interestingly, the detection performance seems to improve with the user speed. This is because speed reduces the size of the communities, which facilitates the task of the community detection step. However, intuition suggests that this trend cannot continue indefinitely since, at some point, assumption (As1) will cease to hold.

To investigate this effect further, Fig. 5 depicts P_D for a given P_{FA} vs. speed. For each frame rate R_J , there is a *critical* speed above which the probability of detection abruptly falls. This effectively constitutes a sharp transition between the regime where (As1) holds and the regime where it does not. Below the critical speed, P_D attains a maximum for a speed that depends on the frame rate.

The experiment in Fig. 6, investigates the influence of the adopted PCD on the spoofing detection performance. The SD algorithm from Sec. III-B is used with the PCD algorithm from Sec. III-A and with the benchmarks. As expected, the better performance of DNNC translates into a better performance in the spoofing detection task.

V. CONCLUSIONS

This work considers the detection of spoofing attacks in wireless networks. RSS features were used since they require no synchronization among receivers and no knowledge about the communication protocol or standard. Due to the high spatial variability of multipath, the proposed detector relies on lower level decisions provided by a position-change detection algorithm. To account for errors in the latter, an algorithm for community detection on graphs is invoked. The sequence of detected communities is then used to decide if a spoofing attack is taking place. To attain high spatio-temporal resolution, a position-change detector was developed based on a DNN. Real data demonstrated that the proposed scheme attains high P_D and low P_{FA} even for small training data sets. Remarkably, acquiring such data is simple since the measurement locations need not be estimated or recorded.

REFERENCES

- [1] C. Koliass, G. Kambourakis, A. Stavrou, and S. Gritzalis, "Intrusion detection in 802.11 networks: empirical evaluation of threats and a public dataset," *IEEE Commun. Surveys & Tutorials*, vol. 18, no. 1, pp. 184–208, 2015.
- [2] M. Vanhoef, C. Matte, M. Cunche, L. S. Cardoso, and F. Piessens, "Why mac address randomization is not enough: An analysis of wi-fi network discovery mechanisms," in *ACM on Asia conf. computer commun. security*, 2016, pp. 413–424.
- [3] J. Martin, D. Alpuche, K. Bodeman, L. Brown, E. Fenske, L. Foppe, T. Mayberry, E. C. Rye, B. Sipes, and S. Teplov, "Handoff all your privacy: A review of apple's bluetooth low energy continuity protocol," *arXiv preprint arXiv:1904.10600*, 2019.
- [4] N. O. Tippenhauer, C. Pöpper, K. B. Rasmussen, and S. Capkun, "On the requirements for successful gps spoofing attacks," in *ACM Conf. Comput. commun. security*, 2011, pp. 75–86.
- [5] V. Brik, S. Banerjee, M. Gruteser, and S. Oh, "Wireless device identification with radiometric signatures," in *Int. Conf. Mobile Comput. Netw.*, 2008, pp. 116–127.
- [6] H. Givehchian, N. Bhaskar, E. R. Herrera, H. R. L. Soto, C. Dameff, D. Bharadia, and A. Schulman, "Evaluating physical-layer ble location tracking attacks on mobile devices," in *IEEE Symp. Security Privacy*. IEEE, 2022, pp. 1690–1704.
- [7] P. Liu, P. Yang, W.-Z. Song, Y. Yan, and X.-Y. Li, "Real-time identification of rogue wifi connections using environment-independent physical features," in *IEEE INFOCOM 2019-IEEE Conf. Computer Commun.* IEEE, 2019, pp. 190–198.
- [8] T. D. Vo-Huu, T. D. Vo-Huu, and G. Noubir, "Fingerprinting wi-fi devices using software defined radios," in *ACM Conf. Security & Privacy Wireless Mobile Netw.*, 2016, pp. 3–14.
- [9] J. Xiong and K. Jamieson, "Secureangle: improving wireless security using angle-of-arrival information," in *ACM SIGCOMM Workshop Hot Topics Netw.*, 2010, pp. 1–6.
- [10] J. Xiong and K. Jamieson, "Securearray: Improving wifi security with fine-grained physical-layer information," in *Annual Int. Conf. Mobile comput. & netw.*, 2013, pp. 441–452.
- [11] X. Shi, B. D. O. Anderson, G. Mao, Z. Yang, J. Chen, and Z. Lin, "Robust localization using time difference of arrivals," *IEEE Signal Process. letters*, vol. 23, no. 10, pp. 1320–1324, 2016.
- [12] N. Wang, L. Jiao, P. Wang, W. Li, and K. Zeng, "Machine learning-based spoofing attack detection in mmwave 60ghz ieee 802.11 ad networks," in *IEEE Conf. Computer Commun.* IEEE, 2020, pp. 2579–2588.
- [13] Y. Chen, W. Trappe, and R. P. Martin, "Detecting and localizing wireless spoofing attacks," in *Annual IEEE Commun. Society Conf. sensor, mesh ad hoc commun. netw.* IEEE, 2007, pp. 193–202.
- [14] J. Yang, Y. Chen, W. Trappe, and J. Cheng, "Detection and localization of multiple spoofing attackers in wireless networks," *IEEE Trans. Parallel Distributed Systems*, vol. 24, no. 1, pp. 44–58, 2012.
- [15] L. Xiao, Y. Li, G. Han, G. Liu, and W. Zhuang, "Phy-layer spoofing detection with reinforcement learning in wireless networks," *IEEE Trans. Vehicular Tech.*, vol. 65, no. 12, pp. 10037–10047, 2016.
- [16] K. Zeng, K. Govindan, D. Wu, and P. Mohapatra, "Identity-based attack detection in mobile wireless networks," in *IEEE INFOCOM*. IEEE, 2011, pp. 1880–1888.
- [17] B. Alotaibi and K. Elleithy, "A new mac address spoofing detection technique based on random forests," *Sensors*, vol. 16, no. 3, pp. 281, 2016.
- [18] M. T. Hoang, Y. Zhu, B. Yuen, T. Reese, X. Dong, T. Lu, R. Westendorp, and M. Xie, "A soft range limited k-nearest neighbors algorithm for indoor localization enhancement," *IEEE Sensors Journal*, vol. 18, no. 24, pp. 10208–10216, 2018.
- [19] A. Sobehy, E. Renault, and P. Mühlethaler, "Csi-mimo: K-nearest neighbor applied to indoor localization," in *IEEE Int. Conf. Commun.* IEEE, 2020, pp. 1–6.
- [20] I. Goodfellow, Y. Bengio, and A. Courville, *Deep Learning*, MIT press, 2016.
- [21] E. D. Kolaczyk, *Statistical Analysis of Network Data: Methods and Models*, Springer, New York, 2009.
- [22] V. D. Blondel, J.-L. Guillaume, R. Lambiotte, and E. Lefebvre, "Fast unfolding of communities in large networks," *Journal stat. mechanics: theory experiment*, vol. 2008, no. 10, pp. P10008, 2008.
- [23] S. M. Kay, *Fundamentals of Statistical Signal Processing, Vol. II: Detection Theory*, Prentice-Hall, 1998.